Nuclear Inst. and Methods in Physics Research, A 972 (2020) 164124

Contents lists available at ScienceDirect

Nuclear Inst. and Methods in Physics Research, A

journal homepage: www.elsevier.com/locate/nima

Characterization of boron-coated silicon sensors for thermal neutron detection

Shruti Mehendale [a,*], Kalliopi Kanaki [c], Marco Povoli [b], Andreas Tefre Samnøy [a], Ganesh Tambave [a], Angela Kok [b], Carina Höglund [c,g], Susann Schmidt [c,h], Saima Sultana Kazi [d], Isabel Llamas-Jansa [d], Thomas Kittelmann [c], Chung-Chuan Lai [c], Thor-Erik Hansen [b], Stanislav Pospíšil [e], Tomáš Slavíček [e], Dieter Röhrich [a], Richard Hall-Wilton [c,f]

[a] Institute of Physics and Technology, University of Bergen, Bergen, Norway
[b] MiNa Lab, SINTEF, Oslo, Norway
[c] European Spallation Source ERIC, P.O. 176, 22 100, Lund, Sweden
[d] IFE, Kjeller, Norway
[e] Czech Technical University, Prague, Czech Republic
[f] Università degli Studi di Milano-Bicocca, Piazza della Scienza 3, 20126 Milano, Italy
[g] Impact coatings AB, Westmansgaten SE-582 16, Linköping, Sweden
[h] Ionbond Switzerland -Olten, Industriestrasse 211, CH-4600, Olten, Switzerland

ARTICLE INFO

Keywords:
Geant4 simulations
Thermal neutron detection
Semiconductor detector
Boron10

ABSTRACT

Silicon neutron detectors can operate at low voltage and come with ease of fabrication and the possibility of integration of readout electronics and thus are attractive from an application point of view. In this paper, we have studied thermal neutron capture by silicon diodes coated with boron carbide (B_4C). One of the surfaces of the diodes was covered with either natural B_4C ($^{nat}B_4C$) or with enriched B_4C ($^{en}B_4C$). We have investigated: (a) the effect of increase in the sensitive area of the surface of the diode covered with B_4C on the neutron detection efficiency and (b) the effect of enrichment of ^{10}B in B_4C. The difference in ^{10}B in $^{nat}B_4C$ (16 at.% in the deposited film) and $^{en}B_4C$ (79 at.% in the deposited film) leads to about three times increase in detection efficiency of the same detector. For the given experimental conditions, we do not observe a direct relationship between increase in the surface area and the detection efficiency. Energy spectra obtained by Geant4 simulations support the experimental observation of finding no direct relation between increase in the surface area and the detection efficiency.

1. Introduction

In past decades, semiconductor detectors have been regarded as an interesting alternative to be used for thermal neutron detection. As compared to the gaseous or scintillation detectors, semiconductor detectors are compact, lightweight, less expensive to fabricate and able to operate at lower voltage. They can come with integrated readout electronics and provide high spatial resolution. In order to capture a thermal neutron in a solid state detector e.g., a diode, a neutron converter material needs to be in close contact with the detector. This is achieved by either fabricating the detector from a neutron converter semiconductor like BN, LiSe, $LiInSe_2$ [1–3] or depositing a separate layer of neutron converter material on the surface of the diode [4–6]. In the former case, the reaction products are created within the sensitive volume of the diode and generate the signal. In the latter case, reaction products created upon interaction between the neutrons and the neutron converter material, are generated within the layer of sensitive material and have to cross this layer to enter the sensitive volume of the diode in order to be detected [7]. The presented approach for neutron detection uses silicon diodes that are fabricated by well-known technology. The popular choice for neutron converter material to be deposited on the diode have been LiF or B_4C since both $^{10}B(n, \alpha)$ and $^{6}Li(n, \alpha)$ reactions have a significant thermal neutron cross-section (3840 barn and 940 barn respectively [8]) and create reaction products that have high enough energy to be detected over the gamma ray background.

The silicon based neutron detectors may find their potential applications in a variety of fields including neutron imaging [9], nuclear security applications [10,11] etc. An interesting application of boron-coated silicon sensors for thermal neutrons is found in transmission monitors at the European Spallation Source ERIC, (ESS), Lund, Sweden [12]. In the light of the next generation of neutron scattering

* Corresponding author.
E-mail address: shruti.mehendale@uib.no (S. Mehendale).

https://doi.org/10.1016/j.nima.2020.164124
Received 3 October 2019; Received in revised form 24 March 2020; Accepted 7 May 2020
Available online 21 May 2020

instruments, technologically mature silicon sensors could prove appropriate as transmission detectors or in applications where high spatial resolution and high time resolution are necessary. However, a low detection efficiency (typically < 5%) remains a shortcoming [13]. Approaches like stacking the two dimensional detectors [14], modifying the surface area of the detector surface to be coated with neutron sensitive layer by etching geometrical structures on it [5,15], and using three dimensional micro-structures filled with neutron sensitive material [5,16–18] have been used to realize a silicon detector with significant efficiency.

In this paper, we have followed one of these approaches, i.e. to modify the surface of the detector by wet-etching structures on it. We have studied two types of the semiconductor neutron detectors coated with B_4C: (a) a conventional planar detector and (b) a detector with one of its surfaces patterned with inverse pyramidal structures. We wish to investigate the effect of the following parameters on neutron capture: (a) the area covered by B_4C and (b) the enrichment of ^{10}B in the coating on neutron capture. A key part of our study is also to simulate the neutron interaction with the same detectors with Geant4 [19–21], compare it with the experimental results and understand the dependence of properties of the detectors, such as the thickness of the neutron converter layer and N doped region (explained in Section 2.1) on the detector response and hence detection efficiency.

2. Experiment

2.1. Detector fabrication

All the detectors have been fabricated as PIN diodes on an n-type Si substrate with a thickness of 300 μm, orientation ⟨100⟩ and resistivity of 10 kΩ cm. Fig. 1(a) and (b) show respectively the schematic diagram of the cross-sectional view of both, conventional planar detector and the detectors with inverse pyramidal structures that have been wet-etched on one of the diode surfaces. After the wet-etching step, two opposite surfaces of the detectors are doped to create a N doped region on the surface with inverse pyramids and P doped region on the opposite face. Both layers have an approximate thickness/depth between 1–2 μm. No metal was deposited on the pyramid side to allow the incoming radiation to reach the conversion region passing through a minimal amount of layers. The patterned metal on the opposite side of the detectors offers electrical contact to the bulk silicon (N-type Si) and to main diode junction (P doped region). These contacts can be used for wire bonding to the PCBs used in testing. More information on the fabrication process and the wet-etching step can be found in [15]. The photograph of one of the detectors mounted on a PCB is shown in Fig. 1(c). The face corresponding to the P doped Si of the detector is visible in the photograph.

In order to increase the area of one of the faces of the diode, one of the two types of inverse pyramid structures were etched on it: (a) pyramids with a rectangular base and (b) with a square base. In case of the pyramids with a rectangular base, the longest dimension of pyramid base is approximately 4.78 mm (the length of the active region is 4.8 mm) and hence the pyramidal structures are wet-etched along a line in only one direction. In this paper we will refer to this type of patterning as one dimensional (1D). On the other hand, in case of patterning with inverse pyramids with square base, an array of inverse pyramids with equal number of structures in X and Y direction has been etched. This type of patterning is referred to as two dimensional (2D) array of pyramids. In this paper, we have studied three detectors: (1) Test Pad: conventional planar detector, (2) Test T35: patterned detector with 1D array of pyramids, with pyramid base 35 μm × 4780 μm and 20 μm gap between the pyramids, 87 pyramids in total, and (3) Test 100: patterned detector with 2D array of pyramids, with pyramid base 85 μm × 85 μm and 15 μm gap between the pyramids, 47 × 47 = 2209 pyramids in total. Table 1 summarizes all the information about the detectors under investigation.

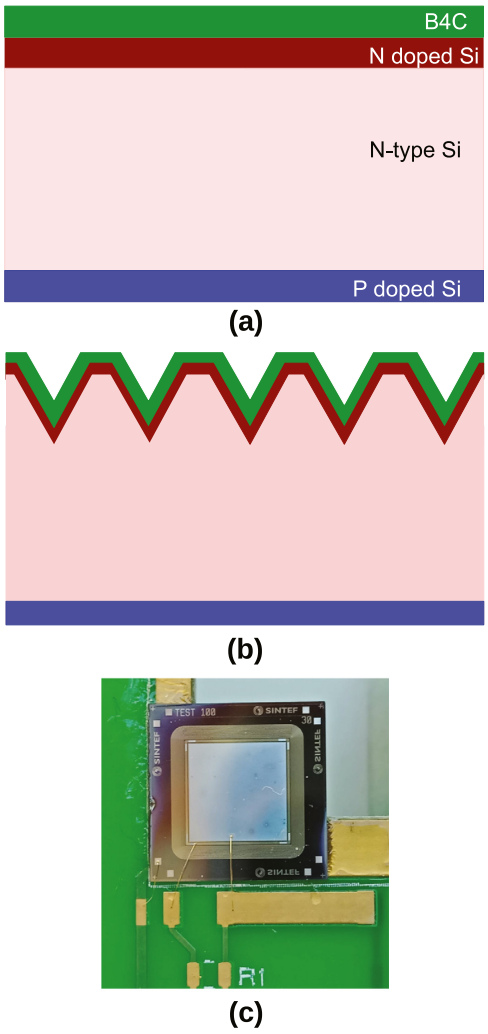

Fig. 1. Schematic diagram of cross-sectional view of the: (a) planar detector, (b) patterned detector, (c) actual photograph of the detector mounted on a PCB.

After wet-etching, the patterned face of the diode was doped with phosphorous by gas phase doping to create an N doped region and the opposite face was doped with boron via ion implantation to create a P doped region. After doping, the side of the detectors corresponding to N doped region was coated with a 400 nm thick layer of either natural B_4C or enriched B_4C by direct current magnetron sputtering (DCMS) from either two natural B_4C (containing approximately 20 at.% of ^{10}B) or two enriched $^{10}B_4C$ (containing approximately 97 at.% of ^{10}B) targets respectively. The deposited films of natural B_4C contain approximately 16 at.% of ^{10}B and those of enriched B_4C contain approximately 79 at.% of ^{10}B. An industrial coating unit (CC800/9, CemeCon AG) located in the ESS Linköping coating workshop was used for the coating process. The machine was evacuated to a base pressure less than 0.5 mPa, then filled up with Ar to 200 mPa prior to the deposition. During the deposition, the substrates were kept at about 190 °C. More details about the coating process can be found in [22–24].

2.2. Detector characterization

I–V (current vs. voltage) and C–V (capacitance vs. voltage) measurements, were carried out after the deposition of the B_4C layer for all the detectors, in order to investigate the leakage current, depletion voltage and capacitance of the PIN diodes. These measurements corresponding to the detector Test 100 coated with enriched B_4C is shown in Fig. 2(a).

Table 1
Information about the topology of the detectors mentioned in this paper; the column surface area denotes the area of that surface of the detector which is coated with B_4C.

Name	Surface structure			Surface area (mm^2)	Neutron converter layer
	Type	Dimension (μm)	Total		
Test pad	Planar	None	0	23	Enriched B_4C 400 nm
Test T35	Inverse pyramid 1D array	35 × 4780 Gap: 20	87	28.67	Enriched B_4C 400 nm
Test 100	Inverse pyramid 2D array	87 × 87 Gap: 15	47 × 47 =2209	28.67	One : enriched B_4C 400 nm Another : standard B_4C 400 nm

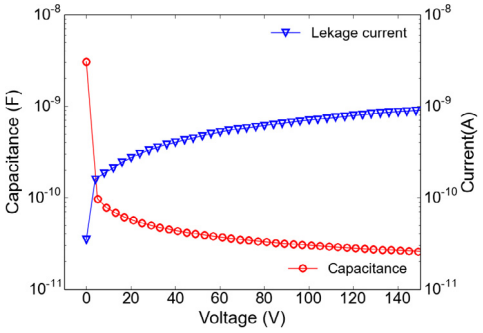

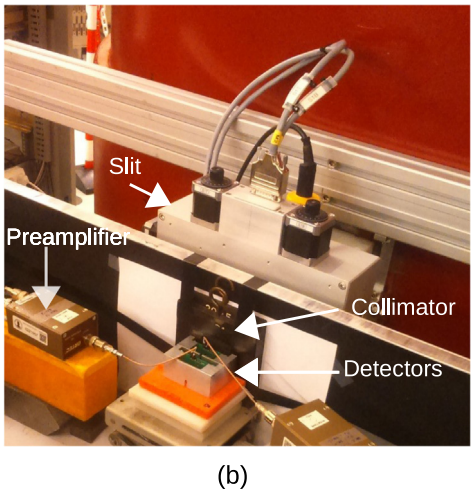

Fig. 2. (a) I–V (current vs. voltage) and C–V (capacitance vs. voltage) measurements corresponding to the detector Test 100 coated with enriched B_4C, (b) photograph of the experimental set-up used at R2D2, IFE, Kjeller, Norway.

The leakage currents were observed to be around 1 nA and the capacitances to be around 36 pF at full depletion voltage of around 60 V for all the detectors mentioned henceforth.

2.3. Experimental set-up for thermal neutron detection

The characterization of the detectors' response to the thermal neutrons was carried out at R2D2 beam-line of JEEPII reactor, IFE, Kjeller, Norway (more information about the beam-line can be found in [12]). During the test, a 2 Å collimated monochromatic beam was used. It was selected from a Bragg reflection from a cubic Ge crystal which acts as a monochromator. It is possible to have the wavelength of the neutron beam from 0.88 Å to 2 Å. The 2 Å wavelength was selected since it has 18% higher intensity than the other wavelengths. The beam size is controlled by a 20 × 20 × 20 × 20 (in mm) slit (JJ X-ray IB-C80-AIR with borated aluminium blades, as indicated in Fig. 2(b)). By doing this, the beam is collimated (FWHM about 1 degree for the 2 Å peak) and is perpendicular to the surface of the detector. In our experimental set-up shown in Fig. 2(b), just next to the slit, a collimator of size 5 mm × 5 mm was kept inside an aluminium dark box, followed by two detectors such that the centres of the detectors were in the path of neutron beam. The thermal neutron flux at the detector was 2.2 × 10^5 neutrons/cm^2 s. It was measured before the experiment by replacing the detectors with a ^{3}He tube (Reuter Stokes — RSP4 0810220) with efficiency of 96.3±0.34% at 2.5 Å.

The bias voltage was kept at 80 V to ensure full depletion of the detectors. The detector output was connected to a charge sensitive pre-amplifier (ORTEC 142) and then to a shaping amplifier (TENNELEC 241) with 0.5 μs shaping time. The shaped signal was further fed to a CAEN ADC (V1729) and VME-PCI Optical Link Bridge (V2718). The neutron beam data was monitored with a software developed at R2D2 beamline, IFE Kjeller and LabVIEW [25] program is used for data acquisition from the detectors. All the measurements were carried out in ambient conditions.

The energy calibration of ADC was done using the 59.54 keV gamma radiated by ^{241}Am. Fig. 3(a) shows the energy spectrum corresponding to the gamma radiation obtained with the same pre-amplifier and amplifier settings as used in all performed experiments. In this spectrum, the first increase in counts, peaking around 100 ADC values was attributed to low energy gammas (26.34 keV and 33.19 keV) radiated by the source. The peak corresponding to 59.54 keV gamma was observed at 222.49 ADC values, leading to a calibration factor of 0.27 keV/ADC channel.

3. Results

3.1. Experimental results

As B_4C is used as the neutron convert material, the corresponding ^{10}B(n, α) reaction is given as:

$$^{10}B + n \rightarrow \alpha\ (1.48\ MeV) + {}^{7}Li\ (0.84\ MeV) + \gamma(0.48\ MeV),$$

excited state (94%)

$$^{10}B + n \rightarrow \alpha\ (1.78\ MeV) + {}^{7}Li(1.02\ MeV),$$

ground state (6%)

Upon interaction between ^{10}B and a thermal neutron in the neutron sensitive layer, the most probable reaction products ^{7}Li (0.84 MeV) and α (1.48 MeV) are emitted in opposite direction and depending on the geometry of the detector, the particle that reaches the sensitive volume of the detector will subsequently be detected. Three main experiments were carried out in order to investigate the following things: (1) neutron capture with B_4C coated layer, (b) effect of enrichment of ^{10}B in the B_4C coating on neutron capture and (c) effect of the patterning the surface of the detector, on neutron capture.

Fig. 3(b) depicts the result from the neutron capture experiment. For this experiment and all the experiments mentioned further, the threshold setting in the ADC was kept so that all the pulses corresponding to energy above 100 keV will be recorded by the ADC. The energy

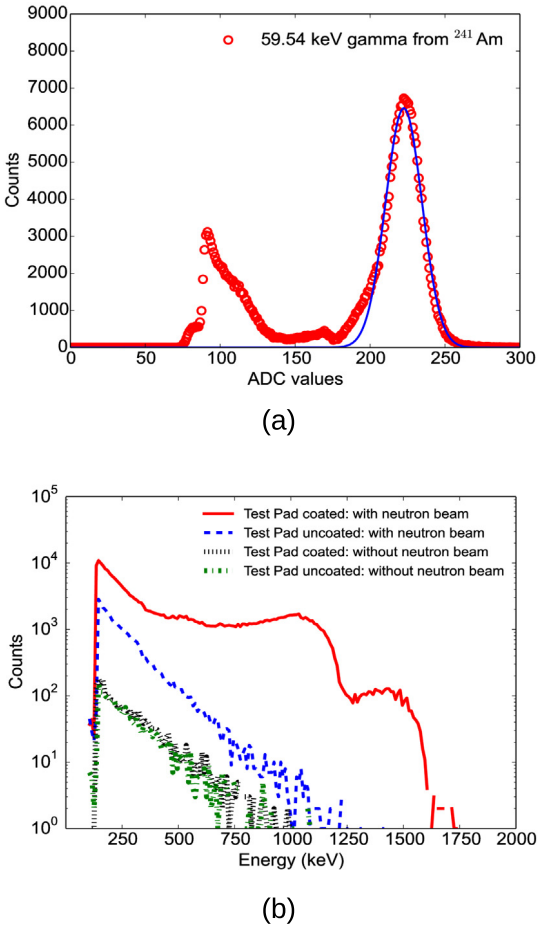

Fig. 3. (a) Energy spectrum obtained from a 59.54 keV gamma emitted from an ^{241}Am source for energy calibration purposes. The blue represents a Gaussian fit to the data, (b) Four energy spectra obtained from planar detector Test Pad: Two from the uncoated detector and two from in presence and absence of the neutron beam, two from the detector coated with enriched B_4C in presence and absence of the neutron beam respectively. (For interpretation of the references to colour in this figure legend, the reader is referred to the web version of this article.)

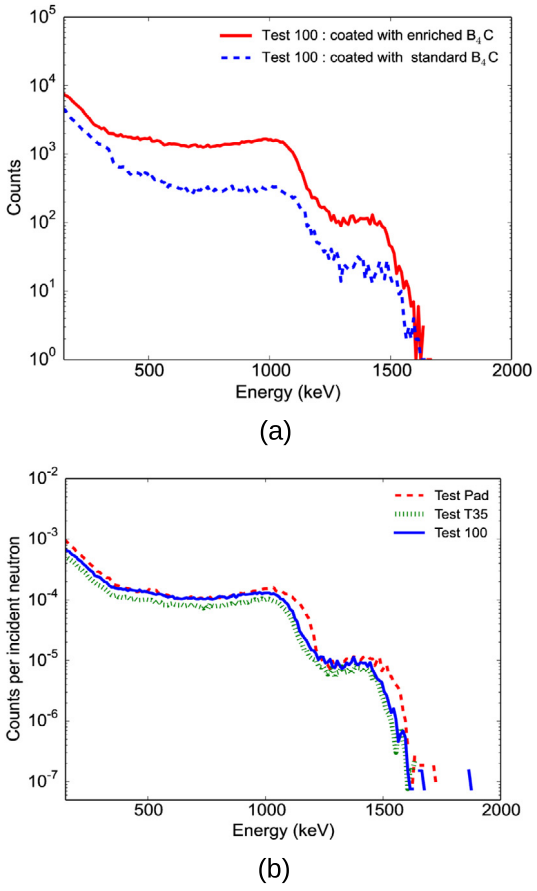

Fig. 4. Experimental results: (a) Effect of ^{10}B enrichment: energy spectra from detectors patterned with a 2D array of inverse pyramids (Test 100) and coated with either natural or enriched B_4C. (b) Effect of patterning: energy spectra obtained from the planar detector Test Pad, the detector patterned with an 1D array of pyramids (Test T35) and the detector patterned with a 2D array of pyramids (Test 100), all coated with enriched B_4C.

spectra obtained from planar diodes, either uncoated or coated with enriched B_4C, in presence and in absence of the neutron beam are shown. The energy spectrum obtained from the planar detector Test Pad coated with enriched B_4C without exposure to the neutron beam gives an idea of the background radiation in absence of the neutron beam. The energy spectrum obtained from the uncoated planar detector Test Pad accounts for the radiation background in Silicon in presence of thermal neutron beam. The clear difference between the energy spectra from planar detectors with and without exposure to the neutron beam indicates neutron capture. According to the ^{10}B(n, α) reaction, one is expected to observe peaks in the energy spectrum at 0.84 MeV (corresponding to ^{7}Li) and at 1.47 MeV or 1.78 MeV (corresponding to α). However, in the energy spectrum shown in Fig. 3(b), the peaks are observed at around 1.05 MeV and 1.45 MeV, which can only be related to the contribution from α. The difference between theoretical and observed values of the peaks correspond to the energy loss experienced by α particles while crossing the layer of B_4C as well as the N doped layer of the detector. This was confirmed by Geant4 simulations, as mentioned in later Section 3.2. Similarly, most of the contribution ^{7}Li (0.84 MeV) is expected to appear at energies lower than 500 keV and it may be rejected by hardware and software threshold settings. Hence, we focus our attention of the energy contribution from the α particles.

The effect of increase in the at.% of ^{10}B in B_4C coating is investigated further. The energy spectra obtained from two identical patterned detectors, namely Test 100, one coated with natural B_4C (with about 16 at.% of ^{10}B in deposited film) and another coated with enriched B_4C (with about 79 at.% of ^{10}B in the deposited film) are shown in Fig. 4(a). Both detectors were simultaneously tested under the neutron beam. As expected, the detector coated with enriched B_4C has more (roughly 3 times) counts corresponding to neutron capture as compared to the detector coated with standard B_4C. The detection efficiency of the detector coated with standard B_4C is $0.08 \pm 0.007\%$ while that of the detector coated with enriched B_4C is $0.28 \pm 0.06\%$ (the number of detected neutrons is counted as the integral of the energy spectra between 300 keV and 2000 keV).

Fig. 4(b) shows the effect of patterning on the surface of the detector on the neutron capture. The energy spectra coming from three detectors coated with enriched B_4C have been compared here. The area of the detector surface covered by B_4C is 23 mm^2 in case of Test Pad while 28.6 mm^2 for both Test T35 and Test 100. Although the increase in area covered by B_4C is about 21%, no increase in the detection efficiency is noticed. The detection efficiency of Test pad, Test 100 and Test T35, all coated with enriched B_4C are $0.32 \pm 0.07\%$ $0.28 \pm 0.06\%$ and $0.21 \pm 0.04\%$ respectively.

Considering the significant uncertainties, the detection efficiencies of the planar and pattered detectors, especially Test Pad and Test 100 are similar while the area covered with B_4C in the latter case is increased by 21%. The main contribution to the error bar comes

Table 2
Experimental detection efficiencies of the detectors tested.

Name	Neutron converter	Detection efficiency
Test pad	Enriched B_4C	$0.32 \pm 0.07\%$
Test T35	Enriched B_4C	$0.21 \pm 0.04\%$
Test 100	Enriched B_4C	$0.28 \pm 0.06\%$
Test 100	Standard B_4C	$0.08 \pm 0.007\%$

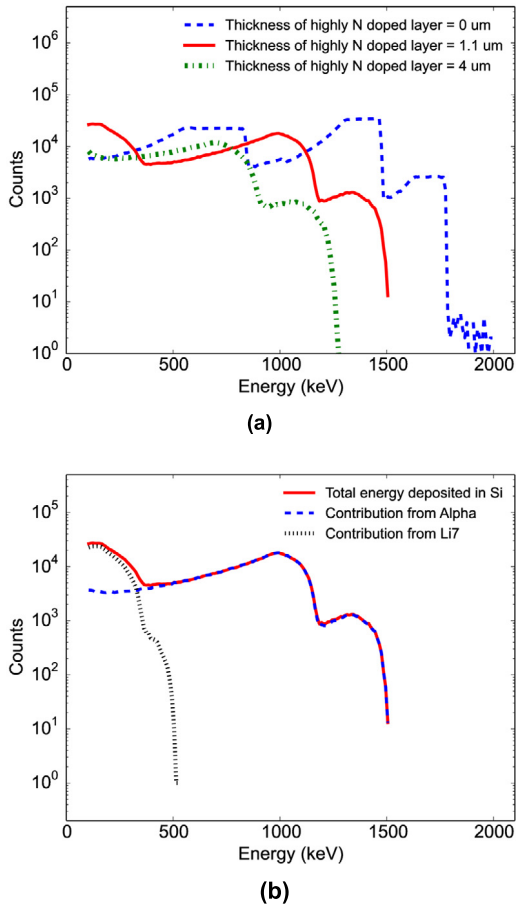

Fig. 5. Geant4 simulations of the neutron interactions inside the planar detector Test Pad coated with enriched B_4C: (a) Effect of the thickness of the N doped layer of the detector on the energy spectrum, (b) The simulated energy deposition spectrum with the thickness of the N doped layer set at 1.1 μm, as well as contributions from different reaction products to the total energy deposited in the detector.

from the uncertainty in the area of the detector exposed to the neutron beam. The size of the collimator (5 mm × 5 mm) and the area of the detector face (4.8 mm × 4.8 mm) are very close. Despite our best efforts of keeping the detectors at exactly the same position for every experiment, slight misalignment in the position of the detector may have led to part of the detector being unexposed to the neutron beam and hence reduction in detection efficiency. The experimental detection efficiencies for all the detectors are given in Table 2

3.2. Geant4 simulations

Geant4 simulations of the neutron interactions with all the detectors studied experimentally were carried out with the ESS simulation framework [26,27] developed by the ESS Detector Group. The Geant4 version used is 10.00.p03 and the physics list is QGSP_BIC_HP.

Each energy spectrum that has been labelled as simulated data has been obtained from simulating 750 million neutrons of wavelength 2 Å falling on to the detector from a rectangular-profile source of dimension 5 mm × 5 mm. The detector was placed in front of the neutron source in such a way that the side with B_4C coating was facing the source. The statistical uncertainty on the simulation results are negligible.

Firstly, in order to understand the energy loss experienced by α particles while crossing the neutron converter and the N doped layer of the detector, Geant4 simulations of the interaction between 1.47 MeV α particles and the detector were carried out. It is observed that the energy deposited by a 1.47 MeV α particle in the sensitive volume of the detector after crossing the B_4C layer of 400 nm thickness and the N doped layer of 1.1 μm thickness is around 1.01 MeV (plot not shown here as the distribution is very narrow), which is in close agreement with the experimental data (see Fig. 3(b)). The difference between the peak energy loss values in the experimental data and the simulations is attributed to the fact that the α particles in the simulation are generated outside the converter and can cross its entirety, while in the experiment the α particles are generated at various locations across the converter depending on the neutron interaction depth [7]. This effect creates different energy deposition profiles.

Since the N doped layer is in between the B_4C layer and the active volume of the diode, the reaction products generated in the $^{10}B(n, \alpha)$ reaction will have to cross the layer (and lose energy while doing so) in order to be detected. Hence, knowing the thickness of this layer is important in order to simulate the detector neutron interaction correctly.

Although all the dimensions of the different layers in the detectors have been specified by the manufacturer, the thickness/depth of the N doped layer (1 μm–2 μm) is not very precise. The uncertainty in the measurement of the thickness stems from the fact that this layer has been doped by gas phase doping and the boundary between doped and un-doped region is not sharp. Hence, the simulations were performed for various thickness of the N doped layer between 0 and 4 μm and the best qualitative match between the simulated and the experimental data was sought. Fig. 5(a) shows the simulated energy spectra for the planar detector Test Pad coated with enriched B_4C with different thickness of the N doped region. As expected, in the absence of this N doped layer (thickness = 0 μm), the peaks corresponding to the α particles are observed at their theoretical values. As the thickness of the layer increases, the peaks are shifted towards lower energies, as expected.

The contributions from different reaction products to the total energy deposited in the active volume of the detector Test Pad coated with enriched B_4C is shown in Fig. 5(b). Here the thickness of the N doped layer is kept at 1.1 μm. It is seen that the two peaks appearing around 1.05 MeV and 1.45 MeV are the result of the energy deposited by the α particles while the ^7Li contribution is mainly visible in the low-energy part of the spectrum (below 500 keV).

3.3. Comparison between experimental and simulated data

The qualitative comparison between the experimental and simulated spectrum for all the three detectors is depicted in Fig. 6. For the plots in this figure, the simulated and experimental spectra have been normalized so that the peaks around 1 MeV, corresponding to α particles, have the same intensity. As mentioned in Section 3.2, the thickness of the N doped region plays a critical role, as far as the peak positions of the simulated energy spectrum are concerned. We have observed that for the planar detector Test pad, the spectrum obtained after simulations with thickness of the N doped region = 1.1 μm matches with the experimental data, as shown in Fig. 6(a). On the other hand, in the case of the patterned detectors, the thickness of the N doped region needs to be kept at 1.5 μm, so as to achieve a qualitative match between the experimental and simulated spectra, as seen in Fig. 6(b) for Test 100 and Fig. 6(c) for Test T35.

The detection efficiency of the sensors and the purity of the recorded signal depend on the energy threshold that is applied. This dependence

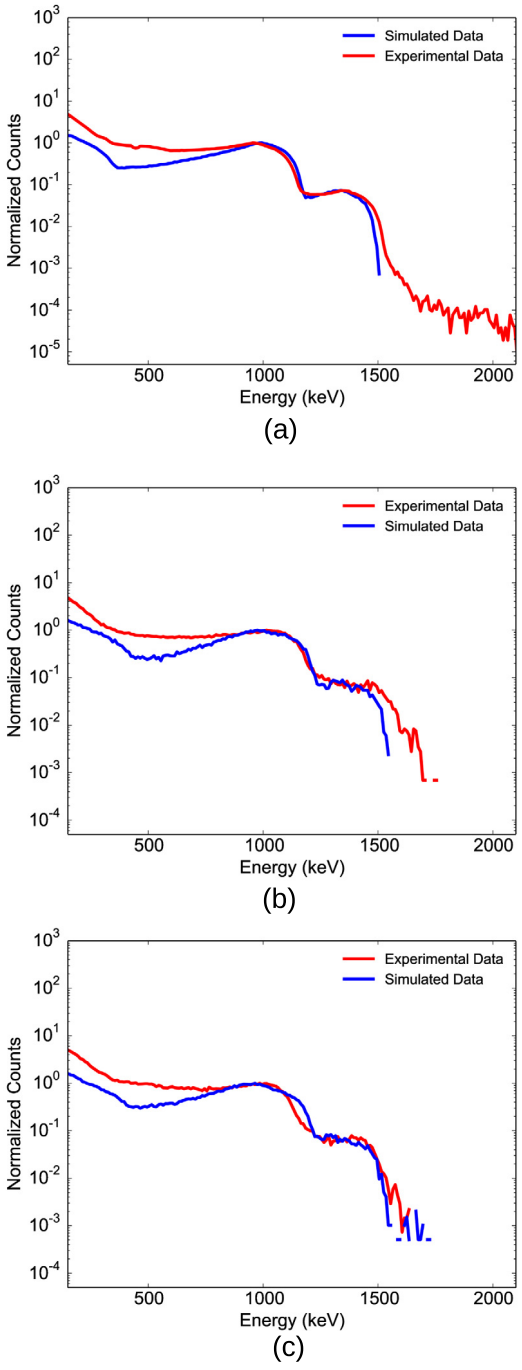

Fig. 6. Comparison between simulated and experimental data:(a) planar detector Test Pad coated with enriched B_4C, simulations are done at thickness of N doped layer = 1.1 μm. (b) patterned detector Test 100 coated with enriched B_4C, simulations are done at thickness of N doped layer = 1.5 μm. (c) patterned detector Test T35 coated with enriched B_4C, simulations are done at thickness of N doped layer = 1.5 μm. The uncertainties are too small to discern.

is depicted in Fig. 7. The simulated efficiency of the Test Pad follows closely the trend of the measured one. In order to fully reject the contribution of the photons to the energy spectrum, a threshold of about 300 keV has to be applied. For that value, the simulated neutron detection efficiency is 0.5% (for 400 nm layer of enriched B_4C) with negligible statistical uncertainty, with respect to the measured one, which is 0.32%. Systematic effects in addition to the thickness of the N doped region, like the thickness uniformity of the converter coating can contribute a 5% effect for an uncertainty of 20 nm, with a larger

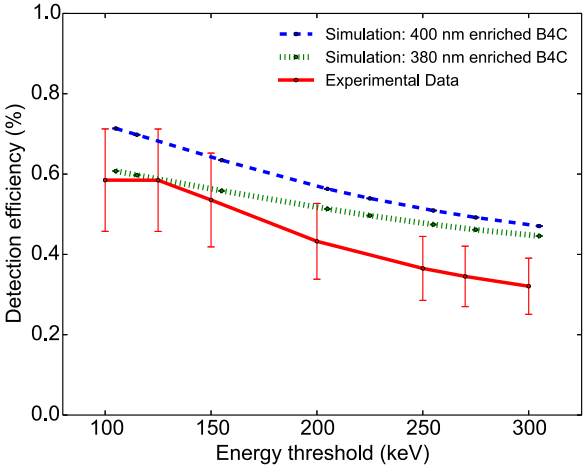

Fig. 7. Test Pad detector : Dependency of experimental and simulated detection efficiency on energy threshold as well as thickness of the neutron converter layer.

effect being present at lower thresholds (see Fig. 7). For the purpose of this work, the level of the quantitative agreement serves the needs of our study.

4. Conclusion

Two types of Si detectors (planar and patterned), coated with either standard or enriched B_4C were tested with a thermal neutron beam. It was observed that planar and patterned detectors coated with just 400 nm thick layer of neutron sensitive material are capable of neutron capture. Enrichment of ^{10}B in the B_4C, for the patterned detector Test 100, leads to an increase in the detection efficiency as expected. While comparing the experimental values of the detection efficiencies of planar and patterned detectors, it is observed that the planar detector Test Pad and patterned detector Test 100 are similar, while Test T35 is the lowest in efficiency even though patterned detectors have about 21% more area covered by B_4C. Although the ^{10}B enrichment leads to an increase in detection efficiency, for the given physical dimensions of the detectors and the experimental conditions, no direct relationship between increase in the area covered by B_4C and detection efficiency was observed. As such it can be concluded that increasing the surface area is not an effective way to improve the neutron detection efficiency unlike the gaseous detectors.

The Geant4 simulations reveal that the thickness of the N doped region plays an important role in determining the shape of the energy spectrum and the main contributions to the simulated energy spectrum come from ^7Li and α particles. The thickness of the N doped region at which simulated and experimental spectra are in qualitative agreement for planar and patterned detectors are different, 1.1 μm and 1.5 μm respectively. As far as the simulated detection efficiencies are concerned, the planar detector has the highest efficiency while Test T35 has the lowest, following the same trend as the experiment. These results show that in order to be able to utilize Silicon detectors, making the doped region very thin is vital.

CRediT authorship contribution statement

Shruti Mehendale: Investigation, Formal analysis, Writing - original draft. **Kalliopi Kanaki:** Conceptualization, Formal analysis, Funding acquisition, Methodology, Software, Writing - review & editing. **Marco Povoli:** Investigation, Formal analysis, Writing - review & editing. **Andreas Tefre Samnøy:** Investigation, Formal analysis, Writing - review & editing. **Ganesh Tambave:** Investigation, Formal analysis, Writing - review & editing. **Angela Kok:** Conceptualization, Funding

acquisition, Investigation, Writing - review & editing. **Carina Höglund:** Investigation, Formal analysis, Writing - review & editing. **Susann Schmidt:** Investigation, Formal analysis, Writing - review & editing. **Saima Sultana Kazi:** Investigation, Formal analysis, Writing - review & editing. **Isabel Llamas-Jansa:** Investigation, Formal analysis, Writing - review & editing. **Thomas Kittelmann:** Formal analysis, Methodology, Software, Writing - review & editing. **Chung-Chuan Lai:** Investigation, Formal analysis, Writing - review & editing. **Thor-Erik Hansen:** Investigation, Formal analysis, Writing - review & editing. **Stanislav Pospíšil:** Investigation, Formal analysis, Writing - review & editing. **Tomáš Slavíček:** Investigation, Formal analysis, Writing - review & editing. **Dieter Röhrich:** Conceptualization, Funding acquisition, Supervision, Writing - review & editing. **Richard Hall-Wilton:** Conceptualization, Funding acquisition, Supervision, Writing - review & editing.

Declaration of competing interest

The authors declare that they have no known competing financial interests or personal relationships that could have appeared to influence the work reported in this paper.

Acknowledgements

This work was funded by the Research Council of Norway under project no. 234234. Computing resources were provided by the DMSC Computing Centre (https://europeanspallationsource.se/data-management-software/computing-centre). Carina Höglund, Kalliopi Kanaki, Thomas Kittelmann, Chung-Chuan Lai, Susann Schmidt and Richard Hall-Wilton would like to acknowledge support from the EU Horizon2020 grant BrightnESS (grant number: 676548).

References

[1] K. Ahmed, R. Dahal, A. Weltz, James J.-Q. Lu, Y. Danon, I.B. Bhat, Solid-state neutron detectors based on thickness scalable hexagonal boron nitride, Appl. Phys. Lett. 110 (2) (2017) 023503, https://doi.org/10.1063/1.4973927.

[2] E. Herrera, D. Hamm, B. Wiggins, R. Milburn, A. Burger, H. Bilheux, L. Santodonato, O. Chvala, A. Stowe, E. Lukosi, LISE pixel detector for neutron imaging, Nucl. Instrum. Methods Phys. Res. A 833 (2016) 142–148, http://www.sciencedirect.com/science/article/pii/S0168900216307768.

[3] E. Tupitsyn, P. Bhattacharya, E. Rowe, L. Matei, M. Groza, B. Wiggins, A. Burger, A. Stowe, Single crystal of LiInSe2 semiconductor for neutron detector, Appl. Phys. Lett. 101 (20) (2012) 202101, https://doi.org/10.1063/1.4762002.

[4] R. Bedogni, D. Bortot, A. Pola, M.V. Introini, M. Lorenzoli, J.M. Gómez-Ros, D. Sacco, A. Esposito, A. Gentile, B. Buonomo, M. Palomba, A. Grossi, Experimental characterization of semiconductor-based thermal neutron detectors, Nucl. Instrum. Methods Phys. Res. A 780 (2015) 51–54, http://www.sciencedirect.com/science/article/pii/S0168900215000893.

[5] J. Uher, 3D Neutron detectors, (Doctoral thesis), Czech Technical University, 2007.

[6] P. Chaudhari, A. Singh, A. Topkar, R. Dusane, Fabrication and characterization of silicon based thermal neutron detector with hot wire chemical vapor deposited boron carbide converter, Nucl. Instrum. Methods Phys. Res. A 779 (2015) 33–38, http://www.sciencedirect.com/science/article/pii/S0168900215000741.

[7] P. Francesco, Boron-10 layers, Neutron Reflectromentry and Thermal Neutron Gaseous Detectors, 2014.

[8] G.F. Knoll, Radiation Detection and Measurement, third ed., John Wiley, New York, 2000.

[9] R. Mendicino, G.-F. Dalla Betta, Three-dimensional detectors for neutron imaging, Nucl. Instrum. Methods Phys. Res. A 878 (2018) 129–140, http://www.sciencedirect.com/science/article/pii/S0168900217308379, Radiation Imaging Techniques and Applications.

[10] S. Ihantola, et al., European reference network for critical infrastructure protection: radiological and nuclear threats to critical infrastructure thematic group: novel detection technologies for nuclear security, eur 29270 en, 2018, http://dx.doi.org/10.2760/703301.

[11] S. Esteban, C. Fleta, C. Guardiola, C. Jumilla, G. Pellegrini, D. Quirion, J. Rodriguez, M. Lozano, Microstructured silicon neutron detectors for security applications, J. Instrum. 9 (12) (2014) C12006, http://stacks.iop.org/1748-0221/9/i=12/a=C12006.

[12] F. Issa, A. Khaplanov, R. Hall-Wilton, I. Llamas, M. Dalseth Riktor, S.R. Brattheim, H. Perrey, Characterization of thermal neutron beam monitors, Phys. Rev. Accel. Beams 20 (2017) 092801, http://dx.doi.org/10.1103/PhysRevAccelBeams.20.092801, https://link.aps.org/doi/10.1103/PhysRevAccelBeams.20.092801.

[13] M. Barbagallo, L. Cosentino, V. Forcina, C. Marchetta, A. Pappalardo, P. Peerani, C. Scirè, S. Scirè, M. Schillaci, S. Vaccaro, G. Vecchio, P. Finocchiaro, Thermal neutron detection using a silicon pad detector and 6lif removable converters, Rev. Sci. Instrum. 84 (3) (2013) 033503, https://doi.org/10.1063/1.4794768.

[14] S.L. Bellinger, R.G. Fronk, T.J. Sobering, D.S. McGregor, High-efficiency microstructured semiconductor neutron detectors that are arrayed, dual-integrated, and stacked, Appl. Radiat. Isot. 70 (7) (2012) 1121–1124, http://www.sciencedirect.com/science/article/pii/S0969804312000140, Proceedings of the 8th International Topical Meeting on Industrial Radiation and Radioisotope Measurement Applications (IRRMA-8).

[15] A. Kok, Z. Kohout, T.-E. Hansen, S. Petersson, S. Pospisil, J. Rokne, T. Slavicek, S. Soligard, G. Thungstrom, Z. Vykydal, Silicon sensors with pyramidal structures for neutron imaging, J. Instrum. 9 (04) (2014) C04011, http://stacks.iop.org/1748-0221/9/i=04/a=C04011.

[16] R. Mendicino, M. Boscardin, S. Carturan, M. Cinausero, G. Collazuol, G.-F. Dalla Betta, M. Dalla Palma, F. Gramegna, T. Marchi, E. Perillo, M. Povoli, A. Quaranta, S. Ronchin, N. Zorzi, Novel 3D silicon sensors for neutron detection, J. Instrum. 9 (05) (2014) C05001, http://stacks.iop.org/1748-0221/9/i=05/a=C05001.

[17] R. Mendicino, M. Boscardin, S. Carturan, G.-F. Dalla Betta, M. Dalla Palma, G. Maggioni, A. Quaranta, S. Ronchin, Characterization of 3D and planar si diodes with different neutron converter materials, Nucl. Instrum. Methods Phys. Res. A 796 (2015) 23–28, http://www.sciencedirect.com/science/article/pii/S0168900215004994, Proceedings of the 10th International Conference on Radiation Effects on Semiconductor Materials Detectors and Devices.

[18] D.S. McGregor, S.L. Bellinger, R.G. Fronk, L. Henson, D. Huddleston, T. Ochs, J.K. Shultis, T.J. Sobering, R.D. Taylor, Development of compact high efficiency microstructured semiconductor neutron detectors, Radiat. Phys. Chem. 116 (2015) 32–37, http://www.sciencedirect.com/science/article/pii/S0969806X15001930, Proceedings of the 9th International Topical Meeting on Industrial Radiation and Radioisotope Measurement Applications.

[19] S. Agostinelli, J. Allison, et al., Geant4 - a simulation toolkit, Nucl. Instrum. Methods A 506 (2003) 250–303.

[20] J. Allison, et al., Geant4 developments and applications, IEEE Trans. Nucl. Sci. 53 (2006) 07.

[21] J. Allison, K. Amako, et al., Recent developments in Geant4, Nucl. Instrum. Methods A 835 (2016) 186–225.

[22] C. Höglund, J. Birch, K. Andersen, T. Bigault, J.-C. Buffet, J. Correa, P. van Esch, B. Guerard, R. Hall-Wilton, J. Jensen, A. Khaplanov, F. Piscitelli, C. Vettier, W. Vollenberg, L. Hultman, B4c thin films for neutron detection, J. Appl. Phys. 111 (10) (2012) 104908, http://dx.doi.org/10.1063/1.4718573, https://doi.org/10.1063/1.4718573.

[23] H. Carina, Z. Karl, K. Petra, J. Jens, G. Grzegorz, L. Jun, H. Lars, B. Jens, H.-W. Richard, Stability of 10b4c thin films under neutron radiation, Radiat. Phys. Chem. 113 (2015) 14–19, http://dx.doi.org/10.1016/j.radphyschem.2015.04.006, http://www.sciencedirect.com/science/article/pii/S0969806X15001449.

[24] S. Schmidt, C. Höglund, J. Jensen, L. Hultman, J. Birch, R. Hall-Wilton, Low-temperature growth of boron carbide coatings by direct current magnetron sputtering and high-power impulse magnetron sputtering, J. Mater. Sci. 51 (23) (2016) 10418–10428, http://dx.doi.org/10.1007/s10853-016-0262-4, https://doi.org/10.1007/s10853-016-0262-4.

[25] LabView software, National Intruments, https://www.ni.com/en-no/shop/labview.html.

[26] T. Kittelmann, I. Stefanescu, K. Kanaki, M. Boin, R. Hall-Wilton, K. Zeitelhack, Geant4 based simulations for novel neutron detector development, J. Phys. Conf. Ser. 513 (2) (2014) 022017.

[27] K. Kalliopi, et al., Simulation tools for detector and instrument design, Physica B 551 (2018) 386–389, http://dx.doi.org/10.1016/j.physb.2018.03.025, http://www.sciencedirect.com/science/article/pii/S0921452618302175, The 11th International Conference on Neutron Scattering (ICNS 2017).